JOURNAL OF COMPUTATIONAL PHYSICS 59, 405–440 (1985)

A Nodal Coarse-Mesh Method for the Efficient Numerical Solution of Laminar Flow Problems

W. C. HORAK

Brookhaven National Laboratory, Department of Nuclear Energy, Upton, New York 11973

AND

J. J. DORNING*

Nuclear Engineering Program, University of Illinois, Urbana, Illinois 61801

Received March 3, 1983; revised July 3, 1984

A coarse-mesh nodal method for the efficient numerical solution of incompressible laminar flow problems is developed using a transverse integration procedure followed by the introduction of locally-defined Green's tensors of the transverse-integrated in-node Navier–Stokes and mass conservation equations. In applications to 2-dimensional flow problems, including fully developed flow, inlet flow, and modified driven cavity problems (driven cavities with inlet and outlet sections), this new nodal Green's tensor method is demonstrated to have very high accuracy even when applied on very large nodes. The high accuracy of this new method on very coarse meshes leads to a high computational efficiency (reduced computer time for fixed accuracy requirements).

1. INTRODUCTION

Accurate calculation of flow fields is an important aspect of the analysis of any thermal hydraulic system. Since the fluid dynamics of such systems are described by a coupled set of nonlinear partial differential equations (usually applied over many heterogeneous regions), the analysis is usually carried out using numerical techniques on a digital computer. In this paper, a new computationally efficient coarse-mesh nodal method, based upon the use of locally defined Green's tensors, is developed and applied to the numerical solution of laminar incompressible fluid flow problems.

Currently, the finite difference method is widely used to numerically solve such problems [1–7]. In the finite difference method, the continuous differential operators in the governing differential equations are replaced by discrete approximate forms of these operators. Thus, the governing differential equations are converted to a set of coupled algebraic equations. This set of coupled algebraic equations is then solved by direct inversion or by an iterative technique.

* Present address: Department of Nuclear Energy, University of Virginia, Charlottesville, Virginia, 22904.

0021-9991/85 $3.00

Two basic approaches exist for the solution of incompressible fluid flow problems by finite difference methods [3]. The first approach uses the stream function and vorticity as the dependent variables. This approach has the advantage that only two variables need be calculated (in two dimensions). Moreover, only one transport equation (for the vorticity) needs to be solved since the stream function equation is a Laplacian. The main disadvantage of this approach is that the velocity distribution is usually desired and this must be constructed numerically from the vorticity and steam function distributions. The boundary conditions are also usually given as specified velocities or specified forces. This usually means that an iterative strategy must be employed to find the boundary conditions in terms of the stream function and vorticity. Moreover, should the pressure distribution be desired, an additional differential equation must be solved numerically. The second approach uses velocity and pressure as the dependent variables. Three variables and two transport equations must be solved as opposed to the two variables and single transport equation in the vorticity-stream function approach. Additionally, the discrete forms of these differential operators sometimes have restrictive stability conditions [3, 7]. Most production computer codes, such as SOLA [6], use velocities and pressure as the principal dependent variables, since this approach tends to be understood more easily by the general user.

In both approaches, difficulties exist in the representation of boundary conditions and the advection term. In most problems, the finite difference method usually requires that variable values actually defined on the interior of the domain be used to approximate values on the system boundary. Thus, the applied boundary conditions will, in general, only be satisfied approximately. The advection term requires the choosing of a velocity from another cell, which in most cases leads to stability restrictions.

Originally applied to the solution of structural mechanics problems [8, 9], the finite element method has since been applied to the solution of fluid flow problems [10, 17]. In finite element analysis, the region of interest is first divided into a set of subdomains (finite elements). The variable(s) of interest are then approximated in terms of a polynomial function with unknown coefficients over the element. A set of coupled algebraic equations for the unknown expansion coefficients is then developed by either minimizing a variational functional or, as is more frequently done, direct application of a weighted residuals procedure. It has been shown that the resulting set of algebraic equations has a direct correspondence to the algebraic set of equations that results from the application of the finite difference method [18, 19]. The main advantages of the finite element method over the finite difference method are in its ease of application to irregular geometries (arbitrary-sided triangular elements have been developed for 2-dimensional applications) and the ability to easily change expansion functions (keeping the order fixed), corresponding to a change of difference schemes in the finite difference method, on an element-by-element basis.

As is the case in finite difference analysis, both the stream function-vorticity [10] and the velocity-pressure [11] formulations have been used in the finite element

analysis of incompressible fluid flow problems. Since the resulting algebraic equations form a nonlinear set in both formulations, an iterative procedure is usually followed in the solution of the algebraic equations.

Finite element methods are capable of satisfying most boundary conditions exactly, but since this severely restricts the choice of expansion functions the boundary conditions are usually satisfied in an approximate weighted residuals sense [17]. The advection term, as in the finite difference method, can require information from other elements for its representation.

While the finite difference method and the finite element method are the two approaches most widely used, mention will be made of three other methods used in the solution of fluid flow problems, since these three methods, like the method developed in this paper, make use of integral equations.

Recently, a numerical method, called the asymmetric separated region weighted residual (ASWR) method, has been developed for the numerical solution of neutron diffusion and fluid flow problems [20–23]. In the ASWR method, the test and weighting functions are defined on nonoverlapping (separated) regions as opposed to weighted residuals in the finite element method in which the test and weighting functions are defined on the same region. Coupling of the regions is obtained by enforcing continuity conditions on the interfaces between regions. The formalism has been developed for 3-dimensional flows and the method applied to the solution of both single phase and two phase transient 1-dimensional fluid flow problems.

A numerical method, called the surface source method, has been developed for the solution of exterior potential fluid flow problems (the method is also applicable to interior flow problems) [24]. In this method, a global Green's function, with Neumann boundary conditions applied at infinity, is used to develop an equation for the flow field in terms of an integral evaluated over the surface of the body immersed in the flow field. This integral equation is then solved by a localized weighted residuals method in which the expansion functions are usually assumed to be constant. Aside from the restriction to potential flow problems, the method can yield (incorrect) results in which flow penetrates the solid boundary and/or is infinite in magnitude.

The boundary element methods are similar to the surface source method. In boundary element methods a global Green's function (usually for the infinite medium) converts the governing differential equation, typically for an interior flow problem, to a global surface integral equation. This global surface problem is then solved using a weighted residuals procedure. Unlike the surface–source method, it can accommodate both Neumann and Dirchlet boundary conditions on the surface [25].

As was the case for the finite element method and the ASWR method, which were originally applied in fields other than fluid mechanics, the method developed in this paper is based in part on two concepts used in the development of high-efficiency computational methods for neutron diffusion problems in fission reactors [26, 27]. In the first application to steady state neutron diffusion problems, locally defined Green's functions were used to convert differential equations applied locally

over subdomains of the system of local multidimensional integral equations [26]. Later, this concept was extended to the solution of steady state and transient heat conduction problems [28, 29]. When these local Green's function methods were improved by combining them with a transverse integration procedure for converting partial differential equations into sets of ordinary differential equations, computational efficiencies one thousand times greater than conventional fully accelerated finite difference method efficiencies were obtained for practical 3-dimensional neutron diffusion problems [27].

In the present method, locally defined Green's tensors of scalar arguments are used to convert a set of ordinary differential equations, obtained by integrating the partial differential equations of fluid flow over one independent variable, to a set of local 1-dimensional integral equations. The "transverse-integrated" velocities and pressure are described by these local integral equations in terms of related quantities defined only on the surfaces of the volume elements. A nonlinear algebraic equation set for the related surface quantities is then developed by evaluating the local integral equations at element surfaces. This nonlinear algebraic equation is solved by a Newton–Raphson procedure. The surface quantities are then substituted into the local integral equations for the transverse-integrated velocities and pressure; finally, these equations are then solved on an element-by-element basis through the application of a local weighted residuals procedure.

2. Formalism

2.1. *Transverse Integration Technique*

To develop a nodal Green's tensor method for 2-dimensional fluid flow problems, we begin by decomposing the system under consideration into a set of L rectangular volume elements, $V_l = (-a_l \leqslant x \leqslant +a_l,\ -b_l \leqslant y \leqslant +b_l)$. We then apply the Navier–Stokes equations and the conservation of mass equation locally over a volume element

$$v_x(x, y)\frac{\partial}{\partial x}v_x(x, y) + v_y(x, y)\frac{\partial}{\partial y}v_x(x, y) - \nu\left(\frac{\partial^2}{\partial x^2}v_x(x, y) + \frac{\partial^2}{\partial y^2}v_x(x, y)\right) + \frac{\partial}{\partial x}p(x, y) = f_x(x, y) \tag{1.a}$$

$$v_x(x, y)\frac{\partial}{\partial x}v_y(x, y) + v_y(x, y)\frac{\partial}{\partial y}v_y(x, y) - \nu\left(\frac{\partial^2}{\partial x^2}v_y(x, y) + \frac{\partial^2}{\partial y^2}v_y(x, y)\right) + \frac{\partial}{\partial y}p(x, y) = f_y(x, y) \tag{1.b}$$

$$\frac{\partial}{\partial x}v_x(x, y) + \frac{\partial}{\partial y}v_y(x, y) = 0. \tag{1.c}$$

This set of equations is then formally made linear by moving the advection terms to the right-hand sides of Eq. (1.a) and Eq. (1.b). The resulting left-hand sides of these equations

$$-\nu\left(\frac{\partial^2}{\partial x^2} v_x(x, y)+\frac{\partial^2}{\partial y^2} v_x(x, y)\right)+\frac{\partial}{\partial x} p(x, y)=f_x(x, y)-(\mathbf{v}(x, y)\cdot\nabla) v_x(x, y)$$

$$=f'_x(x, y) \tag{2.a}$$

$$-\nu\left(\frac{\partial^2}{\partial x^2} v_y(x, y)+\frac{\partial^2}{\partial y^2} v_y(x, y)\right)+\frac{\partial}{\partial y} p(x, y)=f_y(x, y)-(\mathbf{v}(x, y)\cdot\nabla) v_y(x, y)$$

$$=f'_y(x, y) \tag{2.b}$$

$$\frac{\partial}{\partial x} v_x(x, y)+\frac{\partial}{\partial y} v_y(x, y)=0 \tag{2.c}$$

are formally identical to the (linear) Stokes equations.

This set of coupled partial differential equations is then converted to a set of coupled ordinary differential equations through the application of a transverse integration technique. Specifically, we integrate Eqs. (2) in the x direction over the computational node (element) to form

$$-\nu\frac{d^2}{dy^2}\bar{v}_x^x(y)=\bar{S}_1^x(y), \tag{3.a}$$

$$-\nu\frac{d^2}{dy^2}\bar{v}_y^x(y)+\frac{d}{dy}\bar{p}^x(y)=\bar{S}_2^x(y), \tag{3.b}$$

$$\frac{d}{dy}\bar{v}_y^x(y)=\bar{S}_3^x(y), \tag{3.c}$$

where

$$\bar{g}^x(y)=\int_{-a}^{+a} dx\, g(x, y). \tag{4}$$

In matrix form this set of coupled[1] ordinary differential equations becomes,

$$\begin{bmatrix} -\nu\dfrac{d^2}{dy^2} & 0 & 0 \\ 0 & -\nu\dfrac{d^2}{dy^2} & \dfrac{d}{dy} \\ 0 & \dfrac{d}{dy} & 0 \end{bmatrix} \begin{Bmatrix} \bar{v}_x^x(y) \\ \bar{v}_y^x(y) \\ \bar{p}^x(y) \end{Bmatrix} = \begin{Bmatrix} \bar{S}_1^x(y) \\ \bar{S}_2^x(y) \\ \bar{S}_3^x(y) \end{Bmatrix}, \tag{5}$$

[1] Actually, Eq. (3a) is not coupled to the other two equations. However, writing the equations in this form is convenient at this point, and as will be seen, its solution will not depend upon the other equations.

where $\bar{\mathbf{S}}^x(y)$ consists of $\bar{\mathbf{f}}^x(y)$ and the artificial source vector $\bar{\mathbf{Q}}^x(y)$,

$$\begin{Bmatrix} \bar{Q}_1^x(y) \\ \bar{Q}_2^x(y) \\ \bar{Q}_3^x(y) \end{Bmatrix} = \begin{Bmatrix} v \dfrac{\partial}{\partial x} v_x(x, y)\Big|_{-a}^{+a} - p(x, y)\big|_{-a}^{+a} \\ v \dfrac{\partial}{\partial x} v_y(x, y)\Big|_{-a}^{+a} \\ -v_x(x, y)\big|_{-a}^{+a} \end{Bmatrix} \tag{6}$$

which arises from the transverse integration. We now write Eq. (5) in matrix form as

$$\mathbf{A}_x\{\bar{v}^x(y), \bar{p}^x(y)\} = \{\bar{S}^x(y)\}. \tag{7}$$

The development is now repeated to derive analogous equations for the x-dependent, y-integrated quantities. Specifically, we now integrate Eq. (2) in the y direction over the computational node (i.e., volume element or cell) to form

$$-v \frac{d^2}{dx^2} \bar{v}_x^y(x) + \frac{d}{dx} \bar{p}^y(x) = \bar{S}_1^y(x), \tag{8a}$$

$$-v \frac{d^2}{dx^2} \bar{v}_y^y(x) = \bar{S}_2^y(x), \tag{8b}$$

$$\frac{d}{dx} \bar{v}_x^y(x) = \bar{S}_3^y(x), \tag{8c}$$

where,

$$\bar{g}^y(x) = \int_{-b}^{+b} dy\, g(x, y). \tag{9}$$

In this case, the artificial source vector, $\bar{\mathbf{Q}}^y(x)$, which arises from the transverse integration is

$$\begin{Bmatrix} \bar{Q}_1^y(x) \\ \bar{Q}_2^y(x) \\ \bar{Q}_3^y(x) \end{Bmatrix} = \begin{Bmatrix} v \dfrac{\partial}{\partial y} v_x(x, y)\Big|_{-b}^{+b} \\ v \dfrac{\partial}{\partial y} v_y(x, y)\Big|_{-b}^{+b} - p(x, y)\big|_{-b}^{+b} \\ -v_y(x, y)\big|_{-b}^{+b} \end{Bmatrix}. \tag{10}$$

In matrix form, Eq. (8) is written as

$$\mathbf{A}_y\{\bar{\mathbf{v}}^y(x), \bar{p}^y(x)\} = \{\bar{S}^y(x)\}. \tag{11}$$

Thus far, the set of partial differential equations, Eq. (2), has been converted to two sets of ordinary differential equations, Eqs. (7) and (11) through the application of the transverse integration technique.

2.2. *Local Green's Tensor Method Formalism*

2.2.(a) Local integral equations for the transverse-integrated velocities and pressures. A local Green's tensor method is next used to convert the two sets of ordinary differential equations Eqs. (7) and (11) to two sets of local integral equations. Starting with the x-integrated, y-dependent set, Eq. (7), we introduce the adjoint Green's tensor that satisfies,

$$\begin{bmatrix} -\nu\dfrac{d^2}{dy^2} & 0 & 0 \\ 0 & -\nu\dfrac{d^2}{d^2y} & -\dfrac{d}{dy} \\ 0 & -\dfrac{d}{dy} & 0 \end{bmatrix} \times \begin{bmatrix} G^\dagger_{11}(y \mid y_0) & G^\dagger_{12}(y \mid y_0) & G^\dagger_{13}(y \mid y_0) \\ G^\dagger_{21}(y \mid y_0) & G^\dagger_{22}(y \mid y_0) & G^\dagger_{23}(y \mid y_0) \\ G^\dagger_{31}(y \mid y_0) & G^\dagger_{32}(y \mid y_0) & G^\dagger_{33}(y \mid y_0) \end{bmatrix} = \begin{bmatrix} \delta(y-y_0) & 0 & 0 \\ 0 & \delta(y-y_0) & 0 \\ 0 & 0 & \delta(y-y_0) \end{bmatrix}, \tag{12}$$

or in more compact form,

$$\mathbf{A}^\dagger_x \mathbf{G}^\dagger = \delta(y-y_0)\,\mathbf{I}. \tag{13}$$

Multiplying Eq. (7) by $(\mathbf{G}^\dagger)^{\mathrm{T}}$ and Eq. (13) by $\{\bar{\mathbf{v}}^x, \bar{p}^x\}^{\mathrm{T}}$ forms,

$$(\mathbf{G}^\dagger)^{\mathrm{T}}\,\mathbf{A}_x\{\bar{\mathbf{v}}^x, \bar{p}^x\} = (\mathbf{G}^\dagger)^{\mathrm{T}}\,\{\bar{S}^x\}, \tag{14}$$

$$\{\bar{v}^x, \bar{p}^x\}^{\mathrm{T}}\,\mathbf{A}^\dagger_x \mathbf{G}^\dagger = \{\bar{\mathbf{v}}^x, \bar{p}^x\}^{\mathrm{T}}\,\delta(y-y_0)\,\mathbf{I}. \tag{15}$$

Subtracting Eq. (14) from the transpose of Eq. (15), integrating over the node in the y direction, applying Green's theorem, and adding and subtracting the column vector

$$U\{G^\dagger_{1i}(\pm b \mid y_0)\}\,\bar{v}^x_x(\pm b) + U\{G^\dagger_{2i}(\pm b \mid y_0)\}\,\bar{v}^x_y(\pm b), \tag{16}$$

yields,

$$\begin{Bmatrix} \bar{v}_x^x(y_0) \\ \bar{v}_y^x(y_0) \\ \bar{p}^x(y_0) \end{Bmatrix} = \{G_{1i}^\dagger(+b \mid y_0)\}\, J_{\bar{v}_x^x}^{m_y \to l} + \{G_{1i}^\dagger(-b \mid y_0)\}\, J_{\bar{v}_x^x}^{k_y \to l}$$

$$+ \{G_{2i}^\dagger(+b \mid y_0)\}\, J_{\bar{v}_y^x}^{m_y \to l} + \{G_{2i}^\dagger(-b \mid y_0)\}\, J_{\bar{v}_y^x}^{k_y \to l}$$

$$+ \int_{-b}^{+b} dy[\{G_{1i}^\dagger(y \mid y_0)\}\, \bar{S}_1^x(y) + \{G_{2i}^\dagger(y \mid y_0)\}\, \bar{S}_2^x(y_0)\} + \{G_{3i}^\dagger(y \mid y_0)\}\, \bar{S}_3^x(y)] \tag{17}$$

$$- \bar{v}_x^x(+b)\left[U\{G_{1i}^\dagger(+b \mid y_0)\} + \nu \frac{d}{dy}\{G_{1i}^\dagger(y \mid y_0)\}\Big|_{+b} \right]$$

$$- \bar{v}_x^x(-b)\left[U\{G_{1i}^\dagger(-b \mid y_0)\} - \nu \frac{d}{dy}\{G_{1i}^\dagger(y \mid y_0)\}\Big|_{-b} \right]$$

$$- \bar{v}_y^x(+b)\left[U\{G_{2i}^\dagger(+b \mid y_0)\} + \nu \frac{d}{dy}\{G_{2i}^\dagger(y \mid y_0)\}\Big|_{+b} + \{G_{3i}^\dagger(+b \mid y_0)\} \right]$$

$$- \bar{v}_y^x(-b)\left[U\{G_{2i}^\dagger(-b \mid y_0)\} - \nu \frac{d}{dy}\{G_{2i}^\dagger(y \mid y_0)\}\Big|_{-b} - \{G_{3i}^\dagger(-b \mid y_0)\} \right].$$

Here, the y subscripts on the adjacent-element indices m_y and k_y indicate that these indices correspond to the elements immediately above and below (in the y direction) the lth element, and

$$\{G_{ki}^\dagger(y \mid y_0)\} = \begin{Bmatrix} G_{k1}^\dagger(y \mid y_0) \\ G_{k2}^\dagger(y \mid y_0) \\ G_{k3}^\dagger(y \mid y_0) \end{Bmatrix}, \qquad k = 1, 2, 3; \tag{18}$$

U, is a parameter that is introduced in order to handle general boundary conditions (See Sect. 2.4).

At this point in the development of the formalism, a judicious choice for the thus-far unspecified boundary conditions on the adjoint Green's tensor becomes obvious

$$UG_{1i}^\dagger(\pm b \mid y_0) \pm \nu \frac{d}{dy} G_{1i}^\dagger(y \mid y_0)\Big|_{\pm b} = 0, \qquad i = 1, 2, 3, \tag{19}$$

$$UG_{2i}^\dagger(\pm b \mid y_0) \pm \nu \frac{d}{dy} G_{2i}^\dagger(y \mid y_0)\Big|_{\pm b} \pm G_{3i}^\dagger(\pm b \mid y_0) = 0, \qquad i = 1, 2, 3. \tag{20}$$

This choice simplifies Eq. (17) to

$$\begin{Bmatrix} \bar{v}_x^x(y_0) \\ \bar{v}_y^x(y_0) \\ \bar{p}^x(y_0) \end{Bmatrix} = \{G_{1i}^{\dagger}(+b \mid y_0)\}\, J_{\bar{v}_x^x}^{m_y \to l} + \{G_{1i}^{\dagger}(-b \mid y_0)\}\, J_{\bar{v}_x^x}^{k_y \to l}$$
$$+ \{G_{2i}^{\dagger}(+b \mid y_0)\}\, J_{\bar{v}_y^x}^{m_y \to l} + \{G_{2i}^{\dagger}(-b \mid y_0)\}\, J_{\bar{v}_y^x}^{k_y \to l}$$
$$+ \int_{-b}^{+b} dy[\{G_{1i}^{\dagger}(y \mid y_0)\}\, \bar{S}_1^x(y) + \{G_{2i}^{\dagger}(y \mid y_0)\}\, \bar{S}_2^x(y)$$
$$+ \{G_{3i}^{\dagger}(y \mid y_0)\}\, \bar{S}_3^x(y)], \tag{21}$$

where the J quantities are defined on the surfaces of the computational nodes as

$$J_{\bar{v}_x^x}^{m_y \to l} = U\bar{v}_x^x(+b) + \nu \frac{d}{dy}\, \bar{v}_x^x(y)|_{+b}, \tag{22a}$$

$$J_{\bar{v}_x^x}^{k_y \to l} = U\bar{v}_x^x(-b) - \nu \frac{d}{dy}\, \bar{v}_x^x(y)|_{-b}, \tag{22b}$$

$$J_{\bar{v}_y^x}^{m_y \to l} = U\bar{v}_y^x(+b) + \left(\nu \frac{d}{dy}\, \bar{v}_y^x(y)|_{+b} - \bar{p}^x(+b)\right), \tag{22c}$$

$$J_{\bar{v}_y^x}^{k_y \to l} = U\bar{v}_y^x(-b) - \left(\nu \frac{d}{dy}\, \bar{v}_y^x(y)|_{-b} - \bar{p}^x(-b)\right). \tag{22d}$$

The entire development is now repeated for the y-integrated, x-dependent quantities. Thus, Eqs. (11) are converted to a set of local integral equations

$$\begin{Bmatrix} \bar{v}_x^y(x_0) \\ \bar{v}_y^y(x_0) \\ \bar{p}^y(x_0) \end{Bmatrix} = \{G_{1i}^{\dagger}(+a \mid x_0)\}\, J_{\bar{v}_x^y}^{m_x \to l} + \{G_{1i}^{\dagger}(-a \mid x_0)\}\, J_{\bar{v}_x^y}^{k_x \to l}$$
$$+ \{G_{2i}^{\dagger}(+a \mid x_0)\}\, J_{\bar{v}_y^y}^{m_x \to l} + \{G_{2i}^{\dagger}(-a \mid x_0)\}\, J_{\bar{v}_y^y}^{k_x \to l}$$
$$+ \int_{-a}^{+a} dx[\{G_{1i}^{\dagger}(x \mid x_0)\}\, \bar{S}_1^y(x) + \{G_{2i}^{\dagger}(x \mid x_0)\}\, \bar{S}_2^y(x)$$
$$+ \{G_{3i}^{\dagger}(x \mid x_0)\}\, \bar{S}_3^y(x)]. \tag{23}$$

Here the x subscripts on the adjacent-element indices k_x and m_x indicate that these indices correspond to the elements immediately to the left and the right (in the x direction) of the lth element. These J quantities are defined analogously to those in Eqs. (22) as

$$J_{\bar{v}_x^y}^{m_x \to l} = U\bar{v}_x^y(+a) + \left(\nu \frac{d}{dx}\, \bar{v}_x^y(x)\bigg|_{+a} - \bar{p}^y(+a)\right), \tag{24a}$$

$$J^{k_x \to l}_{\bar{v}^y_x} = U\bar{v}^y_x(-a) - \left(\nu \frac{d}{dx} \bar{v}^y_x(x) \Big|_{-a} - \bar{p}^y(-a) \right), \tag{24b}$$

$$J^{m_x \to l}_{\bar{v}^y_y} = U\bar{v}^y_y(+a) + \nu \frac{d}{dx} \bar{v}^y_y(x) \Big|_{+a}, \tag{24c}$$

$$J^{k_x \to l}_{\bar{v}^y_y} = U\bar{v}^y_y(-a) - \nu \frac{d}{dx} \bar{v}^y_y(x) \Big|_{-a}. \tag{24d}$$

Equations (21) and (23) represent two sets of local integral equations which are exact expressions for the directionally integrated velocities and pressures in terms of the J quantities, which are defined only on the surface of the computational node, and a node-volume integral of the total source terms. Expressions are next developed for the J quantities and the total source terms. The elements of the Green's tensors developed here are given in Appendix B.

2.2.(b) Local integral equations for the surface quantities. A set of local integral equations for the J quantities, analogous to Eqs. (21) and (23), are developed using

$$J^{l \to n_y}_{\bar{g}^x} = 2U\bar{g}^x(\pm b) - J^{n_y \to l}_{\bar{g}^x} \tag{25a}$$

and

$$J^{l \to n_x}_{\bar{g}^y} = 2U\bar{g}^y(\pm a) - J^{n_x \to l}_{\bar{g}^y}, \qquad g = v_x, v_y. \tag{25b}$$

This relation is equivalent to stating that the velocities and stresses are continuous at the element interfaces. Evaluating Eq. (21) at the surface yields expressions for the surface velocities which are substituted into Eq. (25a) to form

$$\begin{aligned} J^{l \to m_y}_{\bar{v}^x_x} &= (2UG^{\dagger}_{11}(+b \mid +b) - 1)\, J^{m_y \to l}_{\bar{v}^x_x} \\ &\quad + 2UG^{\dagger}_{11}(-b \mid +b)\, J^{k_y \to l}_{\bar{v}^x_x} \\ &\quad + 2U \int_{-b}^{+b} dy\, G^{\dagger}_{11}(y \mid +b)\, \bar{S}^x_1(y), \end{aligned} \tag{26a}$$

$$\begin{aligned} J^{l \to k_y}_{\bar{v}^x_x} &= 2UG^{\dagger}_{11}(+b \mid -b)\, J^{m_y \to l}_{\bar{v}^x_x} + (2UG^{\dagger}_{11}(-b \mid -b) - 1)\, J^{k_y \to l}_{\bar{v}^x_x} \\ &\quad + 2U \int_{-b}^{+b} dy\, G^{\dagger}_{11}(y \mid -b)\, \bar{S}^x_1(y), \end{aligned} \tag{26b}$$

$$\begin{aligned} J^{l \to m_y}_{\bar{v}^x_y} &= (2UG^{\dagger}_{22}(+b \mid +b) - 1)\, J^{m_y \to l}_{\bar{v}^x_y} \\ &\quad + 2UG^{\dagger}_{22}(-b \mid +b)\, J^{k_y \to l}_{\bar{v}^x_y} \\ &\quad + 2U \int_{-b}^{+b} dy [G^{\dagger}_{22}(y \mid +b)\, \bar{S}^x_2(y) + G^{\dagger}_{32}(y \mid +b)\, \bar{S}^x_3(y)], \end{aligned} \tag{26c}$$

$$J^{l\to k_y}_{\bar v^x_y} = 2UG^{\dagger}_{22}(+b\mid -b)\,J^{m_y\to l}_{\bar v^x_y} + (2UG^{\dagger}_{22}(-b\mid -b)-1)\,J^{k_y\to l}_{\bar v^x_y} + 2U\int_{-b}^{+b} dy[G^{\dagger}_{22}(y\mid -b)\,\bar S^x_2(y) + G^{\dagger}_{32}(y\mid -b)\,\bar S^x_3(y)], \tag{26d}$$

where only the nonzero entries of the adjoint Green's tensor have been included to simplify the expressions.

We next develop analogous expressions for the y-integrated J quantities by evaluating Eq. (23) at the surface and using Eq. (25b),

$$J^{l\to m_x}_{\bar v^y_x} = (2UG^{\dagger}_{11}(+a\mid +a)-1)\,J^{m_x\to l}_{\bar v^y_x} + 2UG^{\dagger}_{11}(-a\mid +a)\,J^{k_x\to l}_{\bar v^y_x} + 2U\int_{-a}^{+a} dx[G^{\dagger}_{11}(x\mid +a)\,\bar S^y_1(x) + G^{\dagger}_{31}(x\mid +a)\,\bar S^y_3(x)], \tag{27a}$$

$$J^{l\to l_x}_{\bar v^y_x} = 2UG^{\dagger}_{11}(+a\mid -a)\,J^{m_x\to l}_{\bar v^y_x} + (2UG^{\dagger}_{11}(-a\mid -a)-1)\,J^{k_x\to l}_{\bar v^y_x} + 2U\int_{-a}^{+a} dx[G^{\dagger}_{11}(x\mid -a)\,\bar S^y_1(x) + G^{\dagger}_{31}(x\mid -a)\,\bar S^y_3(x)], \tag{27b}$$

$$J^{l\to m_x}_{\bar v^y_y} = (2UG^{\dagger}_{22}(+a\mid +a)-1)\,J^{m_x\to l}_{\bar v^y_y} + 2UG^{\dagger}_{22}(-a\mid +a)\,J^{k_x\to l}_{\bar v^y_y} + 2U\int_{-a}^{+a} dx\,G^{\dagger}_{22}(x\mid +a)\,\bar S^y_2(x), \tag{27c}$$

$$J^{l\to k_x}_{\bar v^y_y} = 2UG^{\dagger}_{22}(+a\mid -a)\,J^{m_x\to l}_{\bar v^y_y} + (2UG^{\dagger}_{22}(-a\mid -a)-1)\,J^{k_x\to l}_{\bar v^y_y} + 2U\int_{-a}^{+a} dx\,G^{\dagger}_{22}(x\mid -a)\,\bar S^y_2(x). \tag{27d}$$

Equations (26) and (27) have retained all the important qualities of Eqs. (21) and (23) for the transverse integrated velocities. Specifically, Eqs. (26) and (27) are exact expressions for the J quantities in terms of J quantities on adjacent surfaces and a source term which is operated on by a Green's function volume to surface integral operator.

2.2.(c) Total source term equations. The source terms are now determined by making local, low-order expansions for these terms

$$\bar S^y_i(x) = \sum_{h=1}^{H} \bar s^y_{ih}\,p_{ih}(x), \qquad i=1,2,3, \tag{28a}$$

$$\bar S^x_i(y) = \sum_{h=1}^{H} \bar s^x_{ih}\,p_{ih}(y), \qquad i=1,2,3, \tag{28b}$$

where the P_{ih}'s are Legendre polynomials.

Six equations for the $6H$ unknown expansion coefficients are developed by requiring first that the node-averaged velocities and pressures be consistently calculated from the directionally integrated velocities and pressures and, second, that the forces balance within the node.

To enforce the uniqueness of the node-averaged velocities and pressure, Eq. (21) is integrated over the y direction and Eq. (23) is integrated over the x direction. This yields two sets of expressions for the node-averaged velocities and pressure. These two sets are then set equal to each other to form

$$(b/U)[J^{m_y\to l}_{\bar v^x_x}+J^{k_y\to l}_{\bar v^x_x}]+\int_{-b}^{+b}dy_0\int_{-b}^{+b}dy\,G^{\dagger}_{11}(y\mid y_0)\sum_{h=1}^{H}\bar s^x_{1h}p_{1h}(y)$$
$$=(a/U)[J^{m_x\to l}_{\bar v^y_x}+J^{k_x\to l}_{\bar v^y_x}]+\int_{-a}^{+a}dx_0\int_{-a}^{+a}d_xG^{\dagger}_{11}(x\mid x_0)\sum_{h=1}^{H}\bar s^y_{1h}p_{1h}(x)$$
$$+\int_{-a}^{+a}dx_0\int_{-a}^{+a}dx\,G^{\dagger}_{31}(x\mid x_0)\sum_{h=1}^{H}\bar s^y_{3h}p_{3h}(x), \tag{29a}$$

$$(b/U)[J^{m_y\to l}_{\bar v^x_y}+J^{k_y\to l}_{\bar v^x_y}]+\int_{-b}^{+b}dy_0\int_{-b}^{+b}dy\,G^{\dagger}_{22}(y\mid y_0)\sum_{h=1}^{H}\bar s^x_{2h}p_{2h}(y)$$
$$+\int_{-b}^{+b}dy_0\int_{-b}^{+b}dy\,G^{\dagger}_{32}(y\mid y_0)\sum_{h=1}^{H}\bar s^x_{3h}p_{3h}(y)$$
$$=(a/U)[J^{m_x\to l}_{\bar v^y_y}+J^{k_x\to l}_{\bar v^y_y}]+\int_{-a}^{+a}dx_0\int_{-a}^{+a}dx\,G^{\dagger}_{22}(x\mid x_0)\sum_{h=1}^{H}\bar s^y_{2h}p_{2h}(x), \tag{29b}$$

$$b[-J^{m_y\to l}_{\bar v^x_y}+J^{k_y\to l}_{\bar v^x_y}]+\int_{-b}^{+b}dy_0\int_{-b}^{+b}dy\,G^{\dagger}_{23}(y\mid y_0)\sum_{h=1}^{H}\bar s^x_{2h}p_{2h}(y)$$
$$+\int_{-b}^{+b}dy_0\int_{-b}^{+b}dy\,G_{33}(y\mid y_0)\sum_{h=1}^{H}\bar s^x_{3h}p_{3h}(y)$$
$$=a[-J^{m_x\to l}_{\bar v^y_x}+J^{k_x\to l}_{\bar v^y_x}]+\int_{-a}^{+a}dx_0\int_{-a}^{+a}dx\,G_{13}(x\mid x_0)\sum_{h=1}^{H}\bar s^y_{1h}p_{1h}(x)$$
$$+\int_{-a}^{+a}dx_0\int_{-a}^{+a}dx\,G_{33}(x\mid x_0)\sum_{h=1}^{H}\bar s^y_{3h}p_{3h}(x). \tag{29c}$$

To balance the forces within a node, we integrate Eqs. (2) over the node to form

$$\int_{-a}^{+a}dx\,\bar S^y_1(x)+\int_{-b}^{+b}dy\,\bar S^x_1(y)=\int_{-a}^{+a}\int_{-b}^{+b}dx\,dy\,f'_x(x,y)), \tag{30a}$$

$$\int_{-a}^{+a}dx\,\bar S^y_2(x)+\int_{-b}^{+b}dy\,\bar S^x_2(y)=\int_{-a}^{+a}\int_{-b}^{+b}dx\,dy\,f'_y(x,y), \tag{30b}$$

$$\int_{-a}^{+a}dx\,\bar S^y_3(x)+\int_{-b}^{+b}dy\,\bar S^x_3(y)=0. \tag{30c}$$

Inserting the expansions for the source vectors yields

$$\int_{-a}^{+a} dx \sum_{h=1}^{H} \bar{s}^{y}_{1h} p_{1h}(x) + \int_{-b}^{+b} dy \sum_{h=1}^{H} \bar{s}^{x}_{1h} p_{1h}(y) = \int_{-a}^{+a} \int_{-b}^{+b} dx\, dy\, f'_x(x, y), \quad (31a)$$

$$\int_{-a}^{+a} dx \sum_{h=1}^{H} \bar{s}^{y}_{2h} p_{2h}(x) + \int_{-b}^{+b} dy \sum_{h=1}^{H} \bar{s}^{y}_{2h} p_{2h}(y) = \int_{-a}^{+a} \int_{-b}^{+b} dx\, dy\, f'_y(x, y), \quad (31b)$$

$$\int_{-a}^{+a} dx \sum_{h=1}^{H} \bar{s}^{y}_{3h} p_{3h}(x) + \int_{-b}^{+b} dy \sum_{h=1}^{H} \bar{s}^{x}_{3h} p_{3h}(y) = 0. \quad (31c)$$

For the case $H = 1$, Eqs. (29) and (31) uniquely determine the unknown expansion coefficients for the total source terms in a node in terms of the J quantities on the surfaces of that node. This expansion yields term of order h^3 (Appendix C). A formalism for the case $H = 3$ has been developed in Appendix F of [34]. However, this higher-order approximation has the disadvantage of requiring information from two surfaces of the adjacent nodes, greatly increasing the complexity of the resulting equations, and therefore has not been implemented.

2.2.(d) An alternative local Green's tensor method. A formalism analogous to that developed in Subsection (2.2.a) can be developed directly from Eqs. (1), i.e., with the transverse integration omitted. In that case, for a 2-dimensional problem, the dependent variables remain functions of both position variables, the local integral equations are 2-dimensional equations which include 2-dimensional Green's tensors, and the surface J quantities are functions of the computational-element surface variable. The formal development of this alternative approach is given in Appendix C. Because the final discrete variable equations of this alternative method are more complicated than those that result from the developments of Subsections (2.2.(a)–(c)), this latter formalism has not been implemented here. However, it should be recognized that, although more complex, this alternative method does directly yield more detailed information, viz., the constructed polynomial spatial-dependence of the dependent variables in the interiors of the computational elements.

2.3. *Nonlinear Advection Term*

As mentioned in Section 1, the numerical treatment of the advection term presents certain problems in finite difference and finite element methods. In the nodal Green's tensor method, this nonlinear term appears only in the equations for the total source term. More importantly, since it is the integral of the advection term over the node which appears, it is possible to represent it in terms of the surface quantities through the use of a Green's theorem.

To prove this, we write out the right-hand sides of Eq. (31) to explicitly show the advection term

$$\int_{-a}^{+a}\int_{-b}^{+b} dx\,dy\,f'_x(x,y) = \int_{-a}^{+a}\int_{-b}^{+b} dx\,dy\,f_x(x,y) - \int_{-a}^{+a}\int_{-b}^{+b} dx\,dy(\mathbf{v}(x,y)\cdot\nabla)\,v_x(x,y), \tag{32a}$$

$$\int_{-a}^{+a}\int_{-b}^{+b} dx\,dy\,f'_y(x,y) = \int_{-a}^{+a}\int_{-b}^{+b} dx\,dy\,f_y(x,y) - \int_{-a}^{+a}\int_{-b}^{+b} dx\,dy(\mathbf{v}(x,y)\cdot\nabla)\,v_y(x,y), \tag{32b}$$

Applying Green's theorem to the second volume integral (of the advection term) appearing in Eq. (32) (and using the mass continuity equation) converts it to a surface integral

$$\int_{-a}^{+a}\int_{-b}^{+b} dx\,dy(\mathbf{v}(x,y)\cdot\nabla)\,v_x(x,y) = \int_{-a}^{+a} dx[v_y(x,y)\,v_x(x,y)]\Big|_{-b}^{+b} + \int_{-b}^{+b} dy[v_x^2(x,y)]\Big|_{-a}^{+a}. \tag{33a}$$

Similarly,

$$\int_{-a}^{+a}\int_{-b}^{+b} dx\,dy(\mathbf{v}(x,y)\cdot\nabla)\,v_y(x,y) = \int_{-a}^{+a} dx[v_y^2(x,y)]\Big|_{-b}^{+b} + \int_{-b}^{+b} dy[v_x(x,y)\,v_y(x,y)]\Big|_{-a}^{+a}. \tag{33b}$$

We now approximate the surface velocities by replacing them with their average values on the surfaces. Specifically, we replace the surface integrals on the right-hand sides of Eqs. (33) with

$$\int_{-a}^{+a}\int_{-b}^{+b} dx\,dy(\mathbf{v}(x,y)\cdot\nabla)\,v_x(x,y) \cong [\bar{v}_y^x(y)\,\bar{v}_x^x(y)|_{-b}^{+b}]/(2a) + [\bar{v}_x^y(x)\,\bar{v}_x^y(x)|_{-a}^{+a}]/(2b) \tag{34a}$$

$$\int_{-a}^{+a}\int_{-b}^{+b} dx\,dy(\mathbf{v}(x,y)\cdot\nabla)\,v_y(x,y) \cong [\bar{v}_y^x(y)\,\bar{v}_y^x(y)|_{-b}^{+b}]/(2a) + [\bar{v}_x^y(x)\,\bar{v}_y^y(x)|_{-a}^{+a}]/(2b). \tag{34b}$$

These approximations are developed by expanding the factors in the integrands and truncating those expansions after the leading terms. Finally, we substitute the

definitions of the J quantities in Eqs. (22) and (24) into the right-hand sides of Eqs. (34) forming

$$\int_{-a}^{+a}\int_{-b}^{+b} dx\,dy(\mathbf{v}(x,y)\cdot\nabla)\,v_x(x,y) \cong [\{(J^{m_y\to l}_{\bar v^x_y} + J^{l\to m_y}_{\bar v^x_y})(J^{m_y\to l}_{\bar v^x_x} + J^{l-m_y}_{\bar v^x_x}) - (J^{k_y\to l}_{\bar v^x_y} + J^{l\to k_y}_{\bar v^x_y})(J^{k_y\to l}_{\bar v^x_x} + J^{l\to k_y}_{\bar v^x_x})\}/(2a) + \{(J^{m_x\to l}_{\bar v^x_y} + J^{l\to m_x}_{\bar v^x_y})^2 - (J^{k_x\to l}_{\bar v^x_y} + J^{l\to k_x}_{\bar v^x_y})^2\}/(2b)]/(4U^2) \tag{35a}$$

and

$$\int_{-a}^{+a}\int_{-b}^{+b} dx\,dy(\mathbf{v}(x,y)\cdot\nabla)\,v_y(x,y) \cong [\{(J^{m_y\to l}_{\bar v^x_y} + J^{l\to m_y}_{\bar v^x_y})^2 - (J^{k_y\to l}_{\bar v^x_y} + J^{l\to k_y}_{\bar v^x_y})^2\}/(2a) + \{(J^{m_x\to l}_{\bar v^y_x} + J^{l\to m_x}_{\bar v^y_x})(J^{m_x\to l}_{\bar v^y_y} + J^{l\to m_x}_{\bar v^y_y}) + (J^{k_x\to l}_{\bar v^y_x} + J^{l\to k_x}_{\bar v^y_x})(J^{k_x\to l}_{\bar v^y_y} + J^{l\to k_x}_{\bar v^y_y})\}/(2b)]/(4U^2). \tag{35b}$$

2.4. *Boundary Conditions*

In a fluid system, either the velocities

$$v_n(\pm c, z) = v_{n,0}(z), \tag{36a}$$

$$v_s(\pm c, z) = v_{s,0}(z), \tag{35b}$$

or the stresses

$$-p(\pm c, z) + 2\mu\,\frac{\partial v_n}{\partial n}\bigg|_{\pm c,z} = \sigma_0(z), \tag{37a}$$

$$\mu\left(\frac{\partial v_n}{\partial s} + \frac{\partial v_s}{\partial n}\right)\bigg|_{\pm c,z} = \tau_0(z), \tag{37b}$$

where

$$n = \text{normal direction}$$

$$s = \text{shear direction}$$

$$c = a, b; \qquad z = y, x$$

are specified on a boundary. In practice, it is very difficult to specify the state of stress at a surface and the stress boundary conditions are usually replaced by

$$-p(\pm c, z)+2\mu \left.\frac{\partial v_n}{\partial n}\right|_{\pm c,z} = \sigma_0(z), \tag{38a}$$

$$\mu \left.\frac{\partial v_s}{\partial n}\right|_{\pm c} = \tau_0(z). \tag{38b}$$

For the transversely integrated system, the boundary conditions are taken to be either

$$\bar{v}_n^s(\pm c) = \bar{v}_{n,0}^s \tag{39a}$$

$$\bar{v}_s^s(\pm c) = \bar{v}_{s,0}^s \tag{39b}$$

or

$$-\bar{p}^s(\pm c)+\mu \frac{d}{dn}\bar{v}_n^s(\pm c) = \bar{\sigma}_0^s \tag{40a}$$

$$\mu \frac{d}{dn}\bar{v}_s^s(\pm c) = \bar{\tau}_0^s; \qquad s = y, x;\ c = a, b. \tag{40b}$$

To accommodate these boundary conditions, we define a $J^{k\to l}$ from a fictitious element k, exterior to the system surface. Thus, specified velocities are given by

$$J^{k\to l}_{\bar{v}_n^s} = 2U\bar{v}_{n,0}^s - J^{l\to k}_{\bar{v}_n^s}, \tag{41a}$$

$$J^{k\to l}_{\bar{v}_s^s} = 2U\bar{v}_{s,0}^s - J^{l\to k}_{\bar{v}_s^s}, \tag{41b}$$

and specified "forces" by

$$J^{k\to l}_{\bar{v}_n^s} = 2\bar{\sigma}_0^s + J^{l\to k}_{\bar{v}_n^s}, \tag{42a}$$

$$J^{k\to l}_{\bar{v}_s^s} = 2\tau_0^s + J^{l\to k}_{\bar{v}_s^s}. \tag{42b}$$

Had U been selected to be zero (Sect. 2.2.(a), only the specified velocity (Dirichlet) boundary condition could be handled. Conversely, selecting $1/U = 0$, permits only stress (Neumann) boundary conditions in the formulation. This more general formulation permits both these types of boundary conditions (and if needed, type three or Cauchy boundary conditions) to be handled without changing the Green's tensor on an element basis.

Therefore, in the nodal Green's tensor method the global boundary conditions are represented exactly on the global system surfaces by simple algebraic relationships between J quantities defined on these surfaces. This is in contrast to finite difference where the boundary conditions must frequently be approximated in terms of quantities not defined on the system surface.

2.5. *Solution of the Nodal Green's Tensor Method Equations*

In practice, Eqs. (29) and (31) are used to obtain exact algebraic expressions for the total source term expansion coefficients in terms of the J quantities. These

expressions are then directly substituted into Eqs. (26) and (27). These equations are then combined with the expressions for the specified boundary conditions to form a nonlinear (due to the representation of the advection terms) algebraic equation set solely in terms of the J quantities. This nonlinear algebraic equation set is solved by a Newton–Raphson procedure. The expansion coefficients for the total source terms are then calculated. Finally, the integral expressions for the directionally integrated velocities and pressures are evaluated using a local weighted residuals procedure.

To solve for the J quantities using the Newton–Raphson method, the nonlinear equation set formed by combining Eqs. (26) and (27) with the appropriate boundary conditions is written as

$$f_i(\mathbf{x}) = 0, \tag{43}$$

where

$$x_i = J_i, \qquad i = 1,..., N,$$

N = the number of J quantities to be determined.

Applying the standard Newton–Raphson procedure, Eq. (43) is converted to a series of linear problems of the form

$$0 = \mathbf{f}(\mathbf{x}^n) + \mathbf{J}(\mathbf{x}^{n+1} - \mathbf{x}^n), \tag{44}$$

where

$\mathbf{J}$ is the Jacobian of $\mathbf{f}(\mathbf{x})$,

and

n is the iteration index,

by expanding Eq. (43) in a Taylor series about $\mathbf{x}^{n+1}$. The iterations are terminated when

$$|f_i(\mathbf{x}^n)| \leqslant \varepsilon \tag{45}$$

and

$$\left|\frac{x_i^{n+1} - x_i^n}{x_i^n}\right| \leqslant \varepsilon, \qquad i = 1,..., N. \tag{46}$$

The set of linear equations, Eq. (44), is solved by inverting the Jacobian directly or by using an iterative technique in which J quantities defined on constant y surfaces are determined alternately with the J quantities defined on constant x surfaces.

After the J quantities have been determined, the expansion coefficients for the

total source term are calculated using Eqs. (29) and (31). Equations (21) and (23) are then used to evaluate the directionally integrated velocities and pressure via a local weighted residuals procedure. Independent local, low-order expansions are made for the directionally integrated quantities

$$g(z_0)=\sum_{j=1}^{I} w_j^g\, p_j(z_0), \qquad g=\bar{v}_x^x,\ \bar{v}_y^x,\ \bar{v}_x^y,\ \bar{v}_y^y,\ \bar{p}^x,\ \bar{p}^y, \tag{47}$$

and the expansion coefficients determined. Multiplying each row of Eqs. (21) and (23) by the linearly independent weight functions $u_i(z)$, $i=1,\ldots, I$ and integrating over the node yields

$$[A]\{w\}=\{G_{SV1}\}\, J_h^{k\to l}+\{G_{SV2}\}\, J_h^{m\to l}+\sum_{m=1}^{3}[G_{VVm}]\{\theta_m\}, \tag{48}$$

where

$$\{G_{SV1}\}_i=\int_{-c}^{+c} dz_0\, u_i(z_0)\, G_{st}(-c\mid z_0), \qquad \dim\{G_{SV1}\}=\{I\}, \tag{49}$$

$$\{G_{SV2}\}_i=\int_{-c}^{+c} dz_0\, u_i(z_0)\, G_{st}(+c\mid z_0), \qquad \dim\{G_{SV2}\}=\{I\}, \tag{50}$$

$$[G_{VVm}]_{ij}=\int_{-c}^{+c} dz_0\, u_i(z_0)\int_{-c}^{+c} dz\, p_j(z)\, G_{mt}(z\mid z_0), \qquad \dim[G_{VV}]=[I\times H], \tag{51}$$

$$[A]_{ij}=\int_{-d}^{+d} dz_0\, u_i(z_0)\, q_u(z_0), \qquad \dim[A]=[I\times I], \tag{52}$$

and for

$$g=\bar{v}_x^x\colon\ h=\bar{v}_x^x, \quad z=y, \quad c=b, \quad s=1, \quad t=1, \quad \theta=s^x, \tag{53a}$$

$$g=\bar{v}_y^x\colon\ h=\bar{v}_y^x, \quad z=y, \quad c=b, \quad s=2, \quad t=2, \quad \theta=\bar{s}^x, \tag{53b}$$

$$g=\bar{p}^x\colon\ h=\bar{v}_y^x, \quad z=y, \quad c=b, \quad s=2, \quad t=3, \quad \theta=\bar{s}^x, \tag{53c}$$

$$g=\bar{v}_x^y\colon\ h=\bar{v}_x^y, \quad z=x, \quad c=a, \quad s=1, \quad t=1, \quad \theta=\bar{s}^y, \tag{53d}$$

$$g=\bar{v}_y^y\colon\ h=\bar{v}_y^y, \quad z=x, \quad c=a, \quad s=2, \quad t=2, \quad \theta=\bar{s}^y, \tag{53e}$$

$$g=\bar{p}^y\colon\ h=\bar{v}_x^y, \quad z=x, \quad c=a, \quad s=1, \quad t=3, \quad \theta=\bar{s}^y, \tag{53f}$$

Finally, Eq. (48) is multiplied by $[A]^{-1}$ to generate the local low-order matrix equations that are used on an element-by-element basis to evaluate the local expansion coefficients,

$$\{w\}=\{\tilde{G}_{SV1}\}\, J_h^{k\to l}+\{\tilde{G}_{SV2}\}\, J_h^{m\to l}+\sum_{m=1}^{3}\tilde{G}_{VVm}\{\theta_m\}. \tag{54}$$

Here the tildas indicate that the inverse of the A matrix has been incorporated into the definitions of the G matrices. These equations are entirely local equations and do not involve any long-range coupling. Moreover, the local matrix expressions for the expansion coefficients of the directionally integrated velocities and pressures are independent of each other. Therefore, once the J quantities are determined it is not necessary to evaluate the directionally integrated velocities in order to determine the directionally integrated pressure and vice versa. This independent determination of the directionally integrated velocity and pressure distributions is a very desirable feature of the present method, and does not occur either in most finite element methods for fluid flow problems, in which it is necessary to simultaneously solve for the local expansion coefficients for both the velocity and pressure, or in most finite difference methods using a Laplacian pressure formulation, in which the velocity distribution must be determined before solving for the pressure distribution.

3. Numerical Examples

3.1. *Introduction*

The nodal method developed in the previous section has been applied to the numerical solution of incompressible fluid flow problems. Three sample problems have been solved: (1) fully developed flow between parallel plates, (2) inlet flow between parallel plates, and (3) a modified driven cavity problem. The fully developed flow problem and the modified driven cavity problem were solved for four values of the Reynolds number, Re = 1, 10, 100, 1000; the inlet flow problem was solved only for the Reynolds number, Re = 10. The inlet flow problem and the modified driven cavity problem were also solved using a finite difference, marker and cell, method code, SOLA [6].

[redacted]

the accuracy of a numerical method, it is necessary to establish a reference or benchmark solution. Analytical solutions to the partial differential equations of fluid flow are generally hard to obtain, as was mentioned in Section 1. Therefore, the benchmark solutions are usually generated using numerical procedures.

3.2. *Fully Developed Flow Between Parallel Plates*

A sample fluid flow prblem with fully developed flow between parallel plates was defined in 2-dimensional rectangular geometry. The geometry of the problem and the boundary conditions are shown in Fig. 1. Since the analytic solution is known, the nodal method solution was compared to it rather than to a SOLA generated solution.

To evaluate the accuracy of the nodal Green's tensor method, the global flow region was divided into quadrants of equal area as shown in Fig. 1. The average

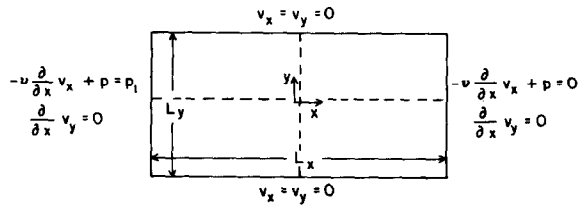

FIG. 1. Geometry and boundary conditions for the fully developed flow problem (showing quadrants over which the velocities were averaged), where $\mathrm{Re} = {}^{v}\max^{L} y/\nu = 1,\ 10,\ 100,\ 1000$; $\nu = 0.01\ \mathrm{cm}^2/\mathrm{s}$; $L_x = 100.\ \mathrm{cm}$; $L_y = 20.\ \mathrm{cm}$; and $P_1 = 1. \times 10^{-5},\ 1. \times 10^{-4},\ 1. \times 10^{-3},\ 1. \times 10^{-2} \mathrm{cm}^2/\mathrm{s}^2$.

x-directed velocity and the average y-directed velocity were then evaluated in each quadrant using the nodal Green's tensor method and the average values compared to the analytic average velocities. This method of comparison thus provides a measure of the average error of the method over large regions while retaining a representation of the local flow distribution.

The problem was solved for four values of the Reynolds number, $\mathrm{Re} = 1,\ 10,\ 100$, and 1000 on four different mesh spacings, 2×2, 4×4, 6×6, and 8×8 elements. In the fully developed flow problem the average quadrant velocities are given by

$$u_{av} = (3.3333 \times 10^{-4}) \times \mathrm{Re}$$

$$v_{av} = 0.0.$$

Additionally, in this problem the average quadrant velocities are identical. In all cases, the nodal Green's tensor method gives the analytic answer to the accuracy of the convergence criterion, $\varepsilon = 10^{-5}$, specified in the numerical procedure. (The calculated node-averaged velocities for every node also agreed with the analytical values to within this accuracy for all the meshes and Reynolds numbers.)

3.3. *Inlet Flow Between Parallel Plates*

A sample fluid flow problem with developing flow at the inlet section between parallel plates was defined in 2-dimensional rectangular geometry. The geometry of the problem and boundary conditions are described in Fig. 2. In this problem the analytic solution is not known in closed form, although approximate solutions

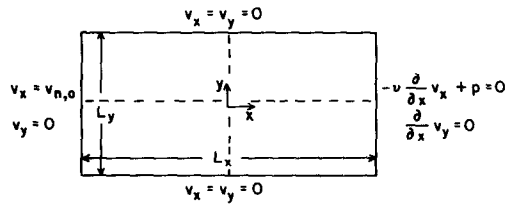

FIG. 2. Geometry and boundary conditions for the inlet flow problem (showing quadrants over which the velocities were averaged), where $\mathrm{Re} = v_{n,0} L_y/\nu = 10$; $\nu = 0.01\ \mathrm{cm}^2/\mathrm{s}$; $L_x = 10.\ \mathrm{cm}$; $L_y = 10.\ \mathrm{cm}$; $v_{n,0} = 0.01\ \mathrm{cm/s}$.

based on boundary layer theory are known. The dimensions of this problem were selected so that the total length of the flow region was approximately twice the entrance length predicted using boundary layer theory [30].

As was the case for the fully developed flow problem, the accuracy was examined by dividing the flow region into quadrants of equal area. Since the analytic solution to this is unknown, reference solutions for these quadrant-average velocities were obtained via a double-Richardson extrapolation of the nodal Green's tensor method results to eliminate the h^2 and h^4 error terms, since analysis of the results generated using the SOLA code showed that they were far from exhibiting an asymptotic h or h^2 error behavior [31]. The results of the calculation for $\mathrm{Re} = 10$ are summarized in Table I, where only two quadrant y-directed velocities are shown, since the problem is symmetric about the centerline and the quadrant-average x-directed velocities were all identical to the reference values (which were also in agreement with the values obtained using boundary layer theory). As shown in Table I, the nodal Green's tensor method obtained accurate results on meshes that are twice as coarse as the SOLA meshes. (The right quadrant velocity values in Table I obtained by the SOLA code are deceptive due to its numerical treatment of the outflow boundary condition. The result of this treatment is that the flow field is forced artificially to have the fully developed pattern even on relatively coarse meshes. The fact that the SOLA results are not yet fully spatially converged is

TABLE I

Comparison of the Results Obtained Using the NGTM for an Inlet Flow Problem for $\mathrm{Re} = 10$ with Those Obtained Using the SOLA Code

	Lower left quadrant		Lower right quadrant		
Mesh	v_y	% error[a]	v_y	% error[a]	CPU(s)[b]
SOLA (Finite Difference Method)					
12×12	0.884×10^{-3}	20.2	1.215×10^{-4}	14.1	4[c]
16×16	0.948×10^{-3}	14.4	1.204×10^{-4}	14.9	15[c]
24×24	1.006×10^{-3}	9.2	1.217×10^{-4}	13.9	100[c]
32×32	1.034×10^{-3}	6.7	1.227×10^{-4}	13.2	250[c]
NGTM (Nodal Green's Tensor Method)					
4×4	0.911×10^{-3}	17.8	0.313×10^{-4}	77.9	0.6
6×6	1.031×10^{-3}	6.9	0.847×10^{-4}	40.1	2.0
8×8	1.065×10^{-3}	3.9	1.095×10^{-4}	22.6	6.0
12×12	1.089×10^{-3}	1.7	1.272×10^{-4}	10.0	30.0[d]
(EXT)[e]	1.108×10^{-3}		1.414×10^{-4}		

[a] Relative to extrapolated answer.
[b] All times for CDC-7600, OPT = 1.
[c] CPU time estimated for specified accuracy of $\varepsilon = 10^{-5}$.
[d] Results obtained from 6×12 half mesh, CPU time is estimate for 12×12 mesh.
[e] $h^2 - h^4$ double-Richardson extrapolation [31].
Note. All results for specified accuracy, $\varepsilon = 10^{-5}$.

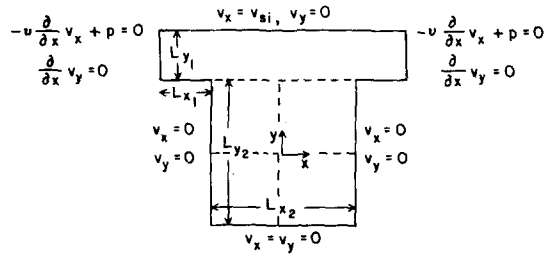

FIG. 3. Geometry and boundary conditions for the modified driven cavity problem (showing quadrants over which the velocities were average), where $\mathrm{Re} = L_{y_2} v_{si}/\nu = L_{x_2} v_{si}/\nu = 1, 100, 100, 1000$; $\nu = 0.01$ cm^2/s; $L_{x_1} = 10.$ cm; $L_{y_1} = 10.$ cm; $L_{x_2} = 20.$ cm; $L_{y_2} = 20.$ cm; $v_s = 5. \times 10^{-4}, 5. \times 10^{-3}, 5. \times 10^{-2}, 5. \times 10^{-1}$ cm/s.

evidenced by the changing left quadrant volicities.) The computing times of this nodal method are much shorter than those of the SOLA code, which was run using its steady state algorithm.

3.4. *Flow in a Modified Driven Cavity*—Re = 1, 10, 100

A sample fluid flow problem for flow in a modified driven cavity was defined in 2-dimensional rectangular geometry. The geometry of the problem and the boundary conditions are shown in Fig. 3. The problem is called a modified driven cavity because of the presence of the inlet and outlet sections at the top of the cavity. The accuracies were examined in this case by dividing only the cavity into quadrants of equal area. The average quadrant velocities were then calculated from the results obtained using the SOLA code on five different meshes, 4×4, 6×6, 8×8, 12×12, and 16×16, with a convergence criterion $\varepsilon = 10^{-10}$. The problem was also solved using the nodal Green's tensor method on four meshes, 2×2, 4×4, 6×6, and 8×8, with a convergence criterion $\varepsilon = 10^{-5}$. Comparison of the computed quadrant velocities showed that while the SOLA results had not yet reached an h^2 convergence rate, the nodal Green's tensor method had obtained this rate. Therefore, in this problem, the reference quadrant velocities were also extrapolated from the nodal Green's tensor method results.

In order to compare the computational efficiency of the two methods, the SOLA code was used to calculate the quadrant average velocities with a convergence criteria of $\varepsilon = 10^{-5}$ on four meshes, 2×2, 4×4, 6×6, and 8×8. The computing times were calculated at all four mesh spacings for both methods. Least-squares fits to linear functions were then made between the logarithm of the average relative error and the logarithm of the number of elements and between the logarithm of the computing time and the logarithm of the number of elements (Fig. 4). A linear relationship was then established between the logarithm of the error and the logarithm of the relative computing time (Fig. 5).

Figure 5 shows the relative computing time as a function of specified average

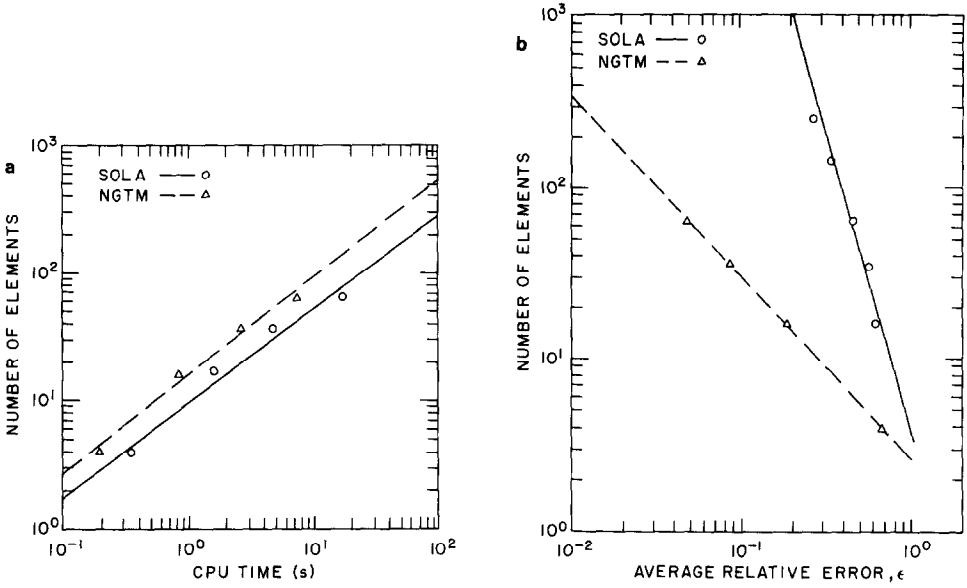

FIG. 4(a). Lest squares fits of the CPU times of SOLA and the NGTM as a function of the number of elements for the modified driven cavity problem Re = 100; (b) Least squares fits of average relative error ε of SOLA and the NGTM as a function of the number of elements for the modified driven cavity problem Re = 100.

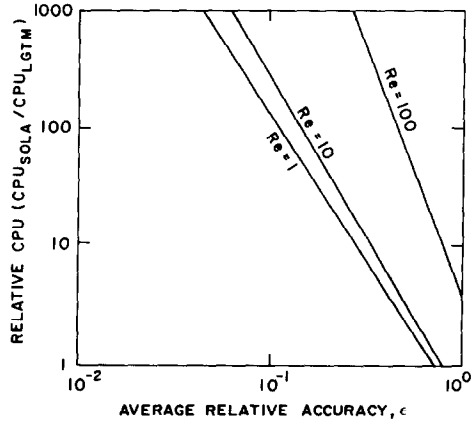

FIG. 5. Relative (CPU) computer time of the nodal Green's tensor method (NGTM) compared to that of the finite-difference code SOLA for the same average relative accuracy of the quadrant-averaged velocity values in the cavity region of a modified driven cavity for three values of the Reynolds number Re.

relative error for three values of the Reynolds number Re = 1, 10, and 100. The advantage in computational efficiency of the nodal Green's tensor method relative to the SOLA code is caused by its high accuracy even on very coarse meshes.

3.5. *Modified-Driven Cavity Problem*—Re = 1000

To further demonstrate the high accuracy of the new method, it was applied to the solution of a modified driven cavity problem with Re = 1000. Figure 6 shows the flow pattern for the cavity region as calculated by the nodal Green's tensor method. The counterflow pattern shown in the lower right-hand corner represents a weak vortex that normally does not appear in the results of finite difference calculations at this Reynolds number unless extremely fine meshes are used [32]. In most methods, it would be necessary to refine the mesh further to fully resolve the vortex motion. In the nodal Green's tensor method, the average surface velocities can be calculated by adding the J quantities defined on the nodal surface. When

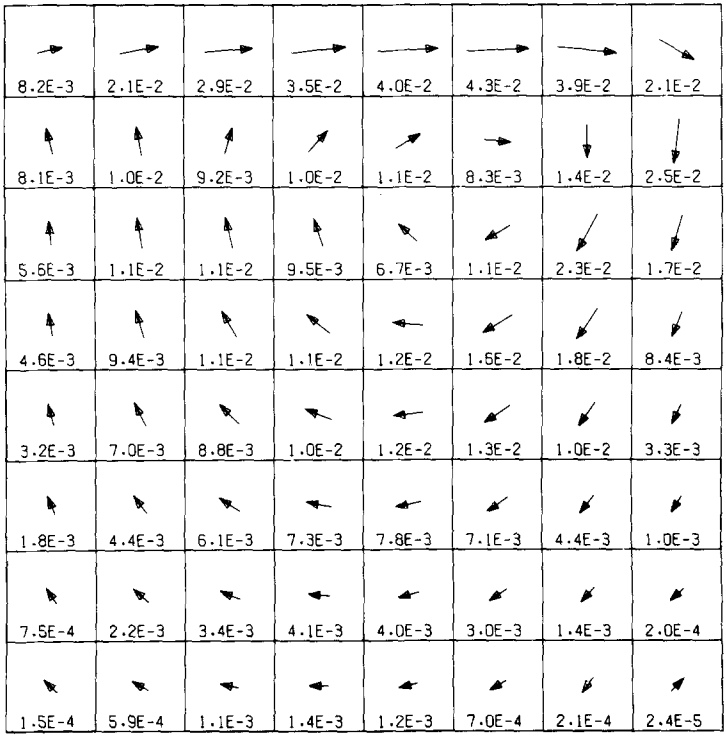

FIG. 6. Flow map of the cavity region of a modified driven cavity calculated using the nodal Green's tensor method on an 8×8 cavity mesh for Reynolds number Re = 1000. Arrows indicate node-averaged velocity magnitudes and directions; numbers indicate node-averaged velocity magnitudes. Note that the counter-flow pattern in lower right corner of cavity is resolved even on this 8×8 mesh.

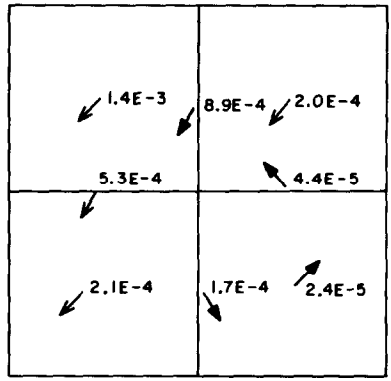

FIG. 7. Surface-average and nodal-average velocities of the four elements in the lower right-hand corner of the cavity region Re = 1000 showing the weak counter-flow vortex pattern.

this is done (effectively halving the mesh), the vortex motion is indeed resolved as shown in Fig. 7, which shows the direction of the surface-average and node-average velocities of the four elements in the lower right-hand corner of the cavity.

4. CONCLUSION

A new numerical method based on the use of local Green's tensors has been developed and applied to the numerical solution of laminar fluid flow problems. This method uses the local Green's tensors to convert a set of ordinary differential equations, obtained through the applications of a transverse integration technique to the coupled Navier–Stokes and conservation of mass equations, to a set of local integral equations. These local integral equations are *exact* expressions for the transverse-integrated velocities and pressures in terms of surface quantities and "total" source terms (which are approximated in terms of the surface quantities). This representation is highly accurate even on very coarse meshes, and leads to vastly greater computational efficiencies compared to more standard methods.

In addition to being computationally more efficient than standard numerical methods, this coarse mesh method also has a simpler and more accurate treatment of boundary conditions than those methods. All boundary conditions for these problems have simple algebraic representations in terms of the *surface*-defined J-quantities as opposed to finite difference methods, where the boundary conditions are frequently approximated by quantities inside the domain rather than on its surface. The advection term is also represented (in conservative form) in terms of the surface J quantities (its effect being propagated over the volume by the Green's integral operators), thus eliminating the difficulties encountered in using the various finite difference representations (and their finite element analogs).

Finally, although the present method is developed in only two dimensions, which

covers a wide range of fluid flow problems, the extension to 3-dimensional calculations, will require no changes in the formalism. Application to 1-dimensional pipe flow, in which some simple problems have already been solved are not reported again here [33, 34], requires a modified formalism.

APPENDIX A: Model Heat Conduction Problem

In order to show in detail the Green's function techniques used in the method developed in this paper and to emphasize the differences between these techniques and more standard methods, such as finite differences, the solution of a 1-dimensional heat conduction problem, using local Green's function techniques and a finite difference control volume formulation, is now presented. More comprehensive presentations of Green's function techniques in the context of heat conduction are given in [28 and 29]. The 1-dimensional heat conduction for Cartesian geometry is given by

$$\frac{d}{dx}\left(k\frac{dT}{dx}\right)+S=0, \tag{A.1}$$

where

k = thermal conductivity

T = temperature

S = volumetric heat source.

We first formulate the control-volume method for this equation. Following the procedure outlined in Patankar [35], we divide the domain into a series of grid points P, which have neighboring points designated E and W (see Fig. A.1). The interfaces between the grid points which define the control volume about the point are designated as x_e and x_w.

Equation (A.1) is now integrated over the finite control volume to form

$$\left(k\frac{dT}{dx}\right)\Big|_{x_e}-\left(k\frac{dT}{dx}\right)\Big|_{x_w}+\int_{x_w}^{x_e} dx\, S=0. \tag{A.2}$$

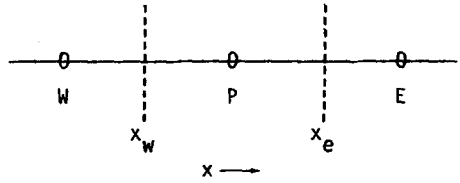

FIG. A.1. Control volume for heat conduction.

The second step is to *assume* an interpolation or profile over the volume. This choice is arbitrary, but the most common is a piece-wise linear profile.

The assumed profile is now used to evaluate the derivatives in Eq. (A.2). Inserting the assumed profiles yields,

$$\frac{k_e(T_E - T_p)}{(x_e - x_p)} - \frac{k_w(T_p - T_w)}{(x_p - x_w)} + \bar{S}\,\Delta x = 0. \tag{A.3}$$

The interface thermal conductivities k_e and k_w must be evaluated in such a manner so as to ensure continuity of the heat flux. The integral of the source term has been replaced by its average over the volume.

Finally, Eq. (A.3) is rearranged to form,

$$a_p T_p = a_E T_E + a_w T_w + b \tag{A.4}$$

where

$$a_E = k_e/(x_e - x_p) \tag{A.5a}$$

$$a_w = k_w/(x_p - x_w) \tag{A.5b}$$

$$a_p = a_E + a_w \tag{A.5c}$$

$$b = \bar{S}\Delta x. \tag{A.5d}$$

This is the final working form of the finite control volume formulation: A discrete pointwise value of the temperature in terms of its neighboring (in this case) pointwise temperatures.

Several comments need to be made on Eq. (A.4):

(1) The equation is in terms of pointwise temperatures not distributions over the control volume. An *approximate* distribution based on the *assumed* profile can be constructed once the grid point values are known.

(2) The values of the coefficients a_p, a_E, and a_w depend directly on the *assumed* profiles.

(3) The nearest-neighbor coupling shown in Eq. (A.2) is dependent on the *assumed* profile. Other profiles could have led to coupling to more distant points.

(4) The interface conductivities k_e and k_w must be evaluated carefully to preserve continuity of the heat flux.

(5) The exact analytic solution to Eq. (A.1) will not, in general, satisfy Eq. (A.4) on a discrete grid.

The development of a local Green's function method for 1-dimensional heat conduction also starts with Eq. (A.1),

$$\frac{d}{dx}\left(k\frac{dT}{dx}\right) + S = 0. \tag{A.1}$$

Next, we introduce the Green's function that satisfies

$$\frac{d}{dx} k \frac{d}{dx} G(x \mid x_0) + \delta(x - x_0) = 0. \tag{A.6}$$

Equation (A.1) is now multiplied by $G(x \mid x_0)$ and Eq. (A.6) by $T(x)$ to form

$$G(x \mid x_0) \frac{d}{dx} k \frac{dT}{dx} + G(x \mid x_0) S = 0 \tag{A.7a}$$

$$T(x) \frac{d}{dx} k \frac{d}{dx} G(x \mid x_0) + T(x) \delta(x - x_0) = 0. \tag{A.7b}$$

Equation (A.7a) is now subtracted from Eq. (A.7b) and the result rearranged to form

$$T(x) \delta(x - x_0) = G(x \mid x_0) \frac{d}{dx} k \frac{dT}{dx} - T(x) \frac{d}{dx} k \frac{d}{dx} G(x \mid x_0) + G(x \mid x_0) S. \tag{A.8}$$

We now integrate Eq. (A.4) over the control volume P, and using Gauss' theorem on the first two terms on the RHS of Eq. (A.4) yields:

$$T^P(x_0) = G(x \mid x_0) k \frac{dT}{dx}\bigg|_{x_e} - G(x \mid x_0) k \frac{dT}{dx}\bigg|_{x_w} + \int_{x_w}^{x_e} dx\, G(x \mid x_0) S^P(x) - \left[T(x) k \frac{dT}{dx} G(x \mid x_0)\bigg|_{x_e} - T(x) k \frac{d}{dx} G(x \mid x_0)\bigg|_{x_w} \right]. \tag{A.9}$$

Equation (A.9) is the standard format for the local Green's function method. Some comparisons with Eqs. (A.4) and (A.9) make clear the very different natures of these two methods:

(1) Equation (A.9) is an *exact* analytic expression of the temperature distribution within a control volume. Equation (A.4), as stated before, is only an approximate equation for a point value of the temperature.

(2) While the first three terms on the RHS of Eq. (A.9) bear a superficial resemblance to Eq. (A.2), the Green's operators in each term relate the surface fluxes and sources to the distribution. Thus, unlike Eq. (A.2) which is an expression of the conservation of energy wiithin the control volume (specifically the heat flux out equals the heat flux in plus the heat deposited directly in the volume), Eq. (A.9) is an expression for the temperature distribution within the cell in terms of the heat fluxes and the heat generated.

(3) Unlike Eq. (A.4), the exact analytic temperature distribution always satisfies Eq. (A.9).

To actually solve Eq. (A.9), we first add and subtract the following two quantities:

$$UG(x \mid x_0)\, T(x)|_{x_e}, \qquad UG(x \mid x_0)\, T(x)|_{x_w}, \tag{A.10}$$

where U is a "fictitious" heat flow resistance (or contact resistance). This parameter is introduced in order to generalize the handling of boundary conditions. Rearranging the resulting equation yields

$$\begin{aligned} T^p(x_0) = & \left\{ G(x \mid x_0) \left[UT(x) + k \frac{d}{dx} T(x) \right] \right\} \Bigg|_{x_e} \\ & + \left\{ G(x \mid x_0) \left[UT(x) - k \frac{d}{dx} T(x) \right] \right\} \Bigg|_{x_w} \\ & - \left\{ T(x_0) \left[UG(x \mid x_0) + k \frac{d}{dx} G(x \mid x_0) \right] \right\} \Bigg|_{x_e} \\ & - \left\{ T(x_0) \left[UG(x \mid x_0) - k \frac{d}{dx} G(x \mid x_0) \right] \right\} \Bigg|_{x_w} \\ & + \int_{x_w}^{x_e} dx\, G(x \mid x_0)\, S^p(x). \end{aligned} \tag{A.11}$$

To simplify Eq. (A.11), we specify the boundary conditions on the Green's function to be

$$\left\{ UG(x \mid x_0) + k \frac{d}{dx} G(x \mid x_0) \right\} \Bigg|_{x_e} = 0 \tag{A.12a}$$

$$\left\{ UG(x \mid x_0) - k \frac{d}{dx} G(x \mid x_0) \right\} \Bigg|_{x_w} = 0 \tag{A.12b}$$

This reduces Eq. (A.11) to

$$\begin{aligned} T^p(x_0) = & \left\{ G(x \mid x_0) \left[UT(x) + k \frac{d}{dx} T(x) \right] \right\} \Bigg|_{x_e} \\ & + \left\{ G(x \mid x_0) \left[UT(x) - k \frac{d}{dx} T(x) \right] \right\} \Bigg|_{x_w} \\ & + \int_{x_e}^{x_w} dx\, G(x \mid x_0)\, S(x). \end{aligned} \tag{A.13}$$

To simplify Eq. (A.13) we define the terms in square brackets as

$$J_e^P = \left[UT(x) + k \frac{d}{dx} T(x) \right] \Big|_{x_e} \tag{A.14a}$$

$$J_w^P = \left[UT(x) - k \frac{d}{dx} T(x) \right] \Big|_{x_w} \tag{A.14b}$$

Equation (A.13) then becomes

$$T^P(x_0) = G(x_e \mid x_0) J_e^P + G(x_w \mid x_0) J_w^P + \int_{x_e}^{x_w} dx\, G(x \mid x_0) S(x). \tag{A.15}$$

Therefore, as shown in Eq. (A.15), if exact analytic expressions for the J-quantities can be obtained, an exact analytic expression for the temperature *distribution* over control volume P is obtained. Such expressions are easily obtained using the following equation:

$$J_e^P = 2UT^E(x_e) - J_w^E \tag{A.16a}$$

$$J_w^P = 2UT^w(x_w) - J_e^w \tag{A.16b}$$

and substituting for the surface temperature the expression given by evaluating Eq. (A.15) at the appropriate surface. The resulting equation is an *exact*, analytic expression for the J's.

The remaining steps for both methods are very similar. The control volume approach yields a tridiagonal matrix in the T_p's, which can be solved easily using standard methods. The T_p's can then be used to find the *approximate* interface values and control volume distribution. The local Green's function method forms a tridiagonal matrix in the J's, which are used to find *exact* interface values and exact control-volume distributions.

APPENDIX B: GREEN'S TENSOR ELEMENTS

$$G_{11}^{\dagger}(y \mid y_0) = \begin{cases} \dfrac{(U(b-y_0)+v)(U(b+y)+v)}{2U(Ub+v)} & -b \leqslant y \leqslant y_0 \\ \dfrac{(U(b+y_0)+v)(U(b-y)+v)}{2U(Ub+v)} & y_0 \leqslant y \leqslant +b \end{cases} \tag{B.1}$$

$$G_{21}^{\dagger}(y \mid y_0) = G_{31}^{\dagger}(y \mid y_0) = 0 \tag{B.2}$$

$$G_{12}^{\dagger}(y \mid y_0) = 0 \tag{B.3}$$

$$G_{22}^{\dagger}(y \mid y_0) = 1./(2U) \tag{B.4}$$

$$G^{\dagger}_{32}(y \mid y_0) = \tfrac{1}{2} \qquad -b \leqslant y \leqslant y_0$$
$$= -\tfrac{1}{2} \qquad y_0 < y \leqslant +b \tag{B.5}$$

$$G^{\dagger}_{13}(y \mid y_0) = 0 \tag{B.6}$$

$$G^{\dagger}_{23}(y \mid y_0) = \tfrac{1}{2} \qquad -b \leqslant y \leqslant y_0$$
$$= -\tfrac{1}{2} \qquad y_0 < y \leqslant +b \tag{B.7}$$

$$G^{\dagger}_{33}(y \mid y_0) = (U/2) + \upsilon\delta(y - y_0) \tag{B.8}$$

$$G^{\dagger}_{11}(x \mid x_0) = 1/(2U) \tag{B.9}$$

$$G^{\dagger}_{21}(x \mid x_0) = 0 \tag{B.10}$$

$$G^{\dagger}_{31}(x \mid x_0) = \tfrac{1}{2} \qquad -a \leqslant x \leqslant x_0$$
$$= -\tfrac{1}{2} \qquad x_0 < x \leqslant +a \tag{B.11}$$

$$G^{\dagger}_{12}(x \mid x_0) = 0.0 \tag{B.12}$$

$$G^{\dagger}_{22}(x \mid x_0) = \begin{cases} \dfrac{(U(a-x_0)+\upsilon)(U(a+x)+\upsilon)}{2U(Ua+\upsilon)} & -a \leqslant x \leqslant x_0 \\ \dfrac{(U(a+x_0)+\upsilon)(U(a-x)+\upsilon)}{2U(Ua+\upsilon)} & x_0 < x \leqslant +a \end{cases} \tag{B.13}$$

$$G^{\dagger}_{32}(x \mid x_0) = 0.0 \tag{B.14}$$

$$G^{\dagger}_{13}(x \mid x_0) = \tfrac{1}{2} \qquad -a \leqslant x \leqslant x_0$$
$$= -\tfrac{1}{2} \qquad x_0 < x < +a \tag{B.15}$$

$$G^{\dagger}_{23}(x \mid x_0) = 0.0 \tag{B.16}$$

$$G^{\dagger}_{33}(x \mid x_0) = (U/2) + \upsilon\delta(x - x_0) \tag{B.17}$$

APPENDIX C: Advection Term Error Analysis

The expansion of the total source terms is the only approximation made in the nodal Green's tensor method. To examine the error this introduces, we follow a procedure developed by Beernick and Dorning [36] for the analysis of neutronics methods.

Starting from the first term on the RHS of Eq. (33), we write,

$$I_1 = \int_{-a}^{+a} dx\, v_y^2(x, y)\Big|_{-b}^{+b} \tag{C.1a}$$

$$= \int_{-a}^{+a} dx\, v_y^2(x, +b) - \int_{-a}^{+a} dx\, v_y^2(x, -b) \tag{C.1b}$$

$$= I_{1,1} + I_{1,2}. \tag{C.1c}$$

We now expand $I_{1,1}$ as

$$I_{1,1} = \int_{-a}^{+a} dx \{ \bar{v}^x_{y,0}(+b)\, p_0(x) + \bar{v}^x_{y,1}(+b)\, p_1(x) + \bar{v}^x_{y,2}(+b)\, p_2(x) + \cdots \}^2, \tag{C.2}$$

where $p_n(x) = p_n(x, a) =$ standard Legendre polynomials, (C.3a)

$$v_y(x, +b)) = \sum_{n=0}^{N} \bar{v}^x_{y,n}(+b)\, p_n(x) \tag{C.3b}$$

$$\bar{v}^x_{y,n} = [(2n+1)/2a] \int_{-a}^{+a} v_y(x, a)\, p_n(x)\, dx \tag{C.3c}$$

and

$$\int_{-a}^{+a} p_n(x)\, p_m(x)\, dx = [2a/(2n+1)]\, \delta_{n,m} \tag{C.3d}$$

We now expand the square brackeeted term in Eq. (C.2), using Eq. (C.3d) to eliminate the cross terms,

$$\begin{aligned} I_{1,1} &= [\bar{v}^x_{y,0}(+b)]^2 \int_{-a}^{+a} p_0(x)\, p_0(x)\, dx \\ &\quad + 2\bar{v}^x_{y,0}(+b)\, \bar{v}^x_{y,1}(+b) \int_{-a}^{+a} p_0(x)\, p_1(x)\, dx \to 0, \text{ cross term} \\ &\quad + [\bar{v}^x_{y,1}(+b)]^2 \int_{-a}^{+a} p_1(x)\, p_1(x)\, dx \\ &\quad + \cdots + [\text{cross terms and higher order coefficients}] \\ &= [\bar{v}^x_{y,0}(+b)]^2 \{2a\} \\ &\quad + [\bar{v}^x_{y,1}(+b)]\{2a/3\}. \end{aligned} \tag{C.4}$$

Following Beernick and Dorning,

$$\bar{v}^x_{y,1}(+b) \text{ is } O(a), \tag{C.5a}$$

which implies

$$[\bar{v}^x_{y,1}(+b)]^2 \text{ is } O^2 \tag{C.5b}$$

and finally yields

$$[\bar{v}^x_{y,1}(+b)]^2 \{2a/3\} \text{ is } O^3. \tag{C.5c}$$

Therefore,

$$I_{1,1} = [\bar{v}^x_{y,0}(+b)]^2\{2a\} + O(a^3). \tag{C.6a}$$

However,

$$\bar{v}^x_{y,0}(+b) = \frac{1}{2a}\,\bar{v}^x_y(+b) \tag{C.6b}$$

which yields

$$I_{1,1} = \frac{[\bar{v}^x_y(+b)]^2}{2a} + O(a^3). \tag{C.6c}$$

Similar analyses can be done for $I_{1,2}$ and the remaining total source terms.

APPENDIX D: A FULL MULTIDIMENSIONAL LOCAL GREEN'S TENSOR METHOD FOR THE SOLUTION OF LAMINAR FLUID FLOW PROBLEMS

A local Green's tensor method that yields multidimensional polynomial distributions for the velocities and pressure can also be developed. Applying the Navier–Stokes equations (with the velocity vector in the convective term decomposed into $\mathbf{v} = \mathbf{v}^* + (\mathbf{v} - \mathbf{v}^*)$, where $\mathbf{v}^*$ is a reference value),

$$\begin{bmatrix} (v^* \cdot \nabla) - \nu\nabla^2 & 0 & \dfrac{\partial}{\partial x} \\ 0 & (v^* \cdot \nabla) - \nu\nabla^2 & \dfrac{\partial}{\partial y} \\ \dfrac{\partial}{\partial x} & \dfrac{\partial}{\partial y} & 0 \end{bmatrix} \begin{Bmatrix} v_x \\ v_y \\ p \end{Bmatrix} = \begin{Bmatrix} f_x \\ f_y \\ 0 \end{Bmatrix} \tag{D.1}$$

or

$$\mathbf{A}\{v, p\} = \{\mathbf{f}, 0\}. \tag{D.2}$$

The adjoint Green's tensor then satisfies

$$\mathbf{A}^\dagger \mathbf{G}^\dagger = \delta(x - x_0)\,\delta(y - y_0)\,\mathbf{I}, \tag{D.3}$$

where $\mathbf{A}^\dagger$ is the adjoint operator.

After cross-multiplying the two matrix equations by the transpose of $\{\mathbf{v}, p\}$ and

$\mathbf{G}^{\dagger}$, subtracting, integrating over the element, applying Gauss' theorem, adding, and subtracting the following integrals,

$$\int_{S^l} d^2\mathbf{r}[U\{G_{1i}^{\dagger}\}\, v_x(\mathbf{r}^s) + U\{G_{2i}^{\dagger}\}\, v_y(\mathbf{r}^s)], \tag{D.4}$$

and selecting the boundary conditions on the adjoint Green's tensor as

$$(U + \hat{n}^l \cdot \mathbf{v}^*)\{G_{1i}^{\dagger}(\mathbf{r}^s \mid \mathbf{r}_0)\} + \hat{n}^l \cdot [v\nabla\{G_{1i}^{\dagger}(\mathbf{r} \mid \mathbf{r}_0)\}|_{r^s} + \hat{t}\{G_{3}^{\dagger}i(\mathbf{r}^s \mid \mathbf{r}_0)\}] = 0.0 \tag{D.5.a}$$

$$(U + \hat{n}^l \cdot \mathbf{v}^*)\{G_{2i}^{\dagger}(\mathbf{r}^s \mid \mathbf{r}_0) + \hat{n}^l \cdot [v\nabla\{G_{2i}^{\dagger}(\mathbf{r} \mid \mathbf{r}_0)\}|_{r^s} + \hat{j}\{G_{3i}^{\dagger}(\mathbf{r}^s \mid \mathbf{r}_0)\}] = 0.0, \tag{D.5.b}$$

the following set of local multidimensional integral equations is obtained:

$$\begin{Bmatrix} v_x(\mathbf{r}_0) \\ v_y(\mathbf{r}_0) \\ p(\mathbf{r}_0) \end{Bmatrix} = \int_{V^l} d^3\mathbf{r}(\mathbf{G}^{\dagger})^{\mathrm{T}}\, \mathbf{f} + \sum_{m=1}^{M} \int_{S^{l,m}} d^2\mathbf{r}[\{G_{1i}^{\dagger}\}\, J_{v_x}^{m\to l}(\mathbf{r}^s) + \{G_{2i}^{\dagger}\}\, J_{v_y}^{m\to l}(\mathbf{r}^s)], \tag{D.6}$$

where

$$\{G_{k_i}^{\dagger}\} = \begin{Bmatrix} G_{k1}^{\dagger}(\mathbf{r} \mid \mathbf{r}_0) \\ G_{k2}^{\dagger}(\mathbf{r} \mid \mathbf{r}_0) \\ G_{k3}^{\dagger}(\mathbf{r} \mid \mathbf{r}_0) \end{Bmatrix}, \tag{D.7}$$

and,

$$J_{v_q}^{m\to l}(\mathbf{r}^s) = Uv_q(\mathbf{r}^s) + \hat{n}^l \cdot (v\,\nabla v_q(\mathbf{r}) - \hat{k}^l p(\mathbf{r}))|_{r^s}, \qquad q = x, y,\ k = i, j \tag{D.8}$$

and S^l is the surface of element l, $\mathbf{r}_0 \in S^l$, and $\mathbf{r}_0 \in V^l$, n^l is the unit outward normal at $\mathbf{r}^s$ and S^l, M is the number of elements adjacent to l, and $S^{l,m}$ is the surface between elements l and m.

Boundary conditions other than those in Eq. (D.5) could be imposed on the adjoint Green's tensor. For example, the use of infinite medium boundary conditions would make the construction of the adjoint Green's tensor less difficult at the expense of adding terms to the surface integral in Eq. (D.6).

Local integral equations are now developed for the J quantities using the relation

$$J_{v_q}^{l\to m}(\mathbf{r}^s) = 2Uv_q(\mathbf{r}^s) - J_{v_q}^{l\to m}(\mathbf{r}^s) \tag{D.9}$$

and evaluating Eq. (D.6) at the surface.

Equations (D.6) and (D.9) (including the expressions for the boundary con-

ditions) are then solved through the application of a local weighted residuals procedure over the elemental volume and elemental surface, respectively. As was the case in the local Green's function method developed for heat conduction problems [29], the expansion coefficients for the surface J quantities are solved first, either iteratively or by direct inversion. The expansion coefficients for the volume-interior velocities and pressures are then solved element-by-element. Since the source in this case depends on the velocity due to the decomposition of the velocity vector in the convective operator, the source must be updated and the process repeated until the velocities and pressures are converged.

It should be noted that all the quantities on the right-hand side of Eq. (D.6) can be approximated from a converged nodal Green's tensor method solution obtained using the method presented in Sections 2.1 through 2.2(c). Thus, this method could be used in conjunction with the nodal method, after the latter is converged, to obtain point-wise distributions for the velocity and pressure as a single final iteration procedure.

ACKNOWLEDGMENTS

This paper is based in part on the doctoral dissertation of one of the authors (W. C. Horak). The research was partially supported by Brookhaven National Laboratory.

REFERENCES

1. R. D. RICHTMEYER AND K. W. MORTON, "Difference Methods for Initial Value Problems," Interscience, New York, 1967.
2. S. NAKAMURA, "Computational Methods in Engineering and Science," Interscience, New York, 1977.
3. P. J. ROACHE, "Computational Fluid Dynamics," Hermosa, Albuquerque, N. M., 1976.
4. A. A. DORODNITSYN, Review of methods for solving the Navier–Stokes equations, *in* "Proceedings Int. Conf. on Numerical Methos in Fluid Mechanics, No. 1," 1973.
5. H. LOMAX, *AIAA J.* **14** (1976), 512.
6. C. W. HIRT, B. D. NICHOLS, AND N. C. ROMERO, "SOLA-A Numerical Solution Algorithm for Transient Fluid Flows," LA-5852, 1975.
7. R. W. HORNBECK, "Numerical Marching Techniques for Fluid Flows with Heat Transfer," NASA SP-297, 1973.
8. O. C. ZIENKIEWICZ, "The Finite Element Method in Structural and Continuum Mechanics," McGraw–Hill, New York, 1971.
9. H. C. MARTIN AND G. F. CAREY, "Introduction to Finite Element Analysis," McGraw–Hill, New York, 1973.
10. A. J. BAKER, *Int. J. Numer. Methods Eng.*, **6** (1973), 89.
11. C. TAYLOR AND P. HOOD, *Comput. Fluids* **1** (1973), 73.
12. S. L. SMITH AND C. A. BREBBIA, *J. Comput. Phys.* **17** (1975), 235.
13. P. P. LYNN AND K. ALANI, *Int. J. Numer. Methods Eng.* **10** (1976), 809.
14. J. T. ODEN AND L. C. WELLFORD, *AIAA J.* (1972), 1590.
15. D. K. GARTLING, "NACHOS: A Finite Element Computer Program for Incompressible Fluid Flow Problems, Part. 1: Theoretical Background," SAND-77-1333, 1978.

16. D. K. GARTLING, "NACHOS: A Finite Element Computer Program for Incompressible Fluid Flow Problems, Part 2: User's Manual," SAND-77-1334, 1977.
17. J. J. CONNOR AND C. A. BREBBIA, "Finite Element Techniques for Fluid Flow," Newnes, London, 1976.
18. W. H. GRAY AND N. M. SCHNURR, *Comput. Methods Appl. Mech. Eng.* **6** (1975), 243.
19. W. H. GRAY AND G. F. PINDER, *Int. J. Numer. Methods Eng.* **10** (1976), 893.
20. S. LANGENBUCH, W. MAURER, AND W. WERNER, *Nucl. Sci. Eng.* **64** (1977), 508.
21. P. ROMSTEDT AND W. WERNER, *Nucl. Sci. Eng.* **64** (1977), 208.
22. W. WERNER, Higher order methods in fluid dynamics, *in* "Computational Methods in Nuclear Engineering," Williamsburg topical meeting, Vol. 1, p. 1. 1979.
23. U. GRAE AND W. WERNER, Application of the ASWR method to 3D two phase flow problems, *in*
24. J. L. HESS, *Comput. Methods Appl. Mech. Eng.* **5** (1975), 145.
25. C. A. BREBBIA, Fundamentals of boundary elements *in* "New Developments in Boundary Element Methods," (C. A. Brebbia, Ed.), p. 3. CML Publ., Southampton, U. K., 1980.
26. T. J. BURNS, "The Partial Current Balance Method: A Local Green's Function Technique for the Numerical Solution of Multidimensional Neutron Diffusion Problems", Ph.D. thesis, Univ. of Illinois, Urbana, Illinois, 1975. See also, T. J. BURNS AND J. J. DORNING, The partial current balance method: A new computational method for the solution of multi-dimensional neutron diffusion problems, *in* "Proceedings of the Joint NEACRP/CSNI Specialists' Meeting in New Developments in Three-Dimensional Neutron Kinetics and Benchmark Calculations," p. 109, Laboratorium fur Reaktorregelung and Anlagensicherung, Garching, Munich, Germany, 1975.
27. R. D. LAWRENCE, "A Nodal Green's Function Method for Multi-Dimensional Neutron Diffusion Calculations," Ph.D. thesis, Univ. of Illinois, Urbana, 1979. See also, R. D. LAWRENCE AND J. J. DORNING, *Nucl. Sci. Eng.* **76** (1980), 218.
28. W. C. HORAK AND J. J. DORNING, *Nucl. Sci. Eng.* **64** (1977), 192.
29. W. C. HORAK AND J. J. DORNING, A coarse-mesh method for heat flow analysis based upon the use of locally-defined Green's functions, *in* "Num. Meth. in Thermal Problems, 2" (R. W. Lewis, K. Morgan and B. A. Schrefler, Eds.), 515. Pineridge, Swansea, U.K., 1981.
30. H. SCHLICHTING, "Boundary Layer Theory," McGraw–Hill, New York, 1968.
31. W. C. HORAK AND J. J. DORNING, A nodal Green's tensor method for the efficient numerical solution of laminar flow problems, *in* "Num. Meth. in Laminar and Turbulent Flow," (C. Taylor and B. A. Schrefler, Eds.), 103. Pineridge, Swansea, U.K., 1981.
32. SHIH-YU TUANN AND MERVYN D. OLSON, *J. Comput. Phys.* **29** (1978), 1.
33. W. C. HORAK AND J. J. DORNING, *Trans. Amer. Nucl. Soc.* **30** (1978), 215.
34. W. C. HORAK, "Local Green's Function Techniques for the Solution of Heat Conduction and Incompressible Fluid Flow Problems," Ph.D. thesis, Univ. of Illinois, Urbana, 1980.
35. S. V. PATANKAR, "Numerical Heat Transfer and Fluid Flow," McGraw–Hill, New York, 1980.
36. K. P. BEERNICK AND J. J. DORNING, The relationships between the nodal, and moments characteristic, transport methods and their errors, *in* "Advances in Reactor Computations," Salt Lake City, 1984, p. 737.